



HAL
open science

Additive manufacturing of cantilever -from masonry to concrete 3D printing

Paul Carneau, Romain Mesnil, Nicolas Roussel, Olivier Baverel

► To cite this version:

Paul Carneau, Romain Mesnil, Nicolas Roussel, Olivier Baverel. Additive manufacturing of cantilever -from masonry to concrete 3D printing. *Automation in Construction*, 2020, 116, pp.103184. 10.1016/j.autcon.2020.103184 . hal-03026642

HAL Id: hal-03026642

<https://hal.science/hal-03026642>

Submitted on 26 Nov 2020

HAL is a multi-disciplinary open access archive for the deposit and dissemination of scientific research documents, whether they are published or not. The documents may come from teaching and research institutions in France or abroad, or from public or private research centers.

L'archive ouverte pluridisciplinaire **HAL**, est destinée au dépôt et à la diffusion de documents scientifiques de niveau recherche, publiés ou non, émanant des établissements d'enseignement et de recherche français ou étrangers, des laboratoires publics ou privés.

Additive manufacturing of cantilever - from masonry to concrete 3D printing

Paul Carneau^{a,*}, Romain Mesnil^{b,a}, Nicolas Roussel^a, Olivier Baverel^a

^aLaboratoire Navier, UMR 8205, Ecole des Ponts, CNRS, UGE, Champs-sur-Marne, France

^bÉcole des Ponts ParisTech, Marne-La-Vallée, France

Abstract

3d printing of cementitious material is a relatively new additive manufacturing process whose growing interest and fast development is mainly due to the digitalised manufacturing, allowing the disposition of material where it pleases. Yet, due to the properties of the fresh material and the difficulty to generate paths for the robots, the printed geometries have remained simple. In this regard, this paper longs to broaden the range of printable shapes by proposing a process-aware exploration of the 3d printing design space.

This is done by looking at historic strategies that have been developed to build cantilevers, vaults and domes in masonry - a more ancient additive manufacturing process. Similarities and main differences between the two processes are pointed out, at the scale of the component, the layer and the global structure. From that a classification of masonry strategies to build cantilevers is proposed, facilitating the identification of parameters for 3d printing that will allow to reproduce such structures. Later, some guidelines for the design of printable geometries and the generation of robotic toolpaths are given, in the light of previous findings.

Keywords: Cementitious material, concrete 3d printing, masonry, cantilever, vaults, funicularity, digital manufacturing, robotic

1. Introduction

Born with the promise of liberating forms in architecture by using digital manufacturing, 3d printing increasing interest is also guided by cost and time saving opportunities, safety, on-site security, and environmental concerns for optimisation of material and waste reduction. Indeed, the construction industry produces today 35% of solid waste in the world [1], while resources are depleting and population is increasing. These observations bring new challenges for researchers, engineers and architects who have to find new methods for designing, building, using and even recycling structures in the future.

Regarding fabrication with concrete, some solutions

have recently been proposed with new construction systems taking advantage of computation and digital fabrication, such as concrete shell cast onto textile formworks [2] to limit waste produced by fabrication or a printed space truss insulating wall [3] weighing a fraction of conventional building systems in concrete, bringing fabrication awareness and material understanding at the forefront of the design process.

3d printing of concrete or cementitious material can be viewed as a perfect example where the final object is a consequence of the fabrication process. The last decade has seen an increase in research topics related to concrete 3d printing [4] as well as in the apparitions of its commercial applications at a large scale. Houses, columns inspired by organic shapes, walls with specific insulation properties [5], even bridges [6] have been printed, extending each time

*Corresponding author

E-mail: paul.carneau@enpc.fr

the design space associated with the technology.

The goal of this paper is to keep exploring this design space by studying the possibilities of printing cantilevers in concrete or clay without the use of temporary support in order to limit waste and cost of fabrication. The challenge is to identify the constraints specific to the process and deduce the admissible geometries within the specified design space. This work starts by finding inspiration into masonry building techniques, another additive manufacturing process, and adapting its strategies to the material, technology and process that define concrete 3d printing. Moreover we propose an a priori assessment of the printability of complex shapes with respect to the material time window and properties of the pump.

1.1. Challenges

A challenge of mortar 3d printing is to ensure the stability of the object during the whole process *since the extruded material keeps being loaded until the end of the fabrication*. The potential failure modes that can occur have been identified: a global instability of the object, a plastic collapse or a phase change (solid to liquid) and an elastic buckling of the structure. The first mode has been identified by Bhooshan *et al.* in [7] and concerns mainly the geometry of the object. The other two modes shown in Fig. 1 identified by Suiker [8] and Wolfs [9], are also linked to material properties and are thus more difficult to predict, especially for non standard geometries.

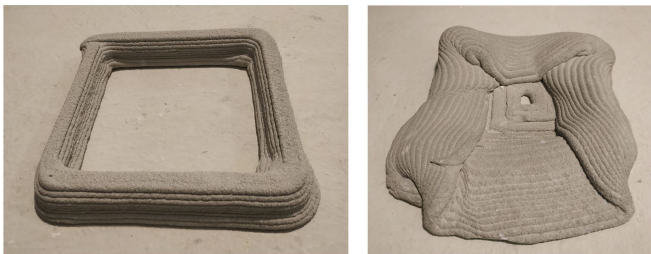


Figure 1: *left*: plastic failure of the lower layers highlighted by the larger width due to the deformations, *right*: buckling collapse of a similar geometry which propagated on the four walls. (Image: Paul Carneau)

When printing cantilevers, the stresses in the material are higher than for a standard vertical wall with potential apparition of tensile stress and bending moment. The risk of failure of the object during the process is increased and the geometry, the material formulation and the printing set-up have to be optimised in order to successfully complete the fabrication.

1.2. Previous works on 3d printing of cantilevers

Additive manufacturing assisted by robot or 3d printing is already used successfully in aeronautics [10] or automotive industry [11] with other materials. Technologies to print metal or plastic have existed for quite a while now. Plastic 3d printing (PLA, ABS, etc.) has emerged at the beginning of twenty-first century, opening the technology of additive manufacturing to the general public. The question of finding the design space of printable geometries has already been worked around with those different materials. Strategies depend on the material used and its short term behaviour, but also on the process itself.

- in Fused Deposition Modelling (FDM), using plastic material (such as PLA or ABS), the most common solution is the real-time fabrication of temporary supports, printed at the same time and with the same material as the final object, and removed afterwards. Algorithms of generation of supports minimising the amount of material used [12], [13], [14], play with parameters such as the maximum inclination of the admissible cantilever, the structure of the supports and its density. Another approach, closer to what is presented in this paper and presented by Allaire and al. in [15], proposes to optimise a printable structure with a level-set method. The topology optimisation algorithm prevents cantilevers in the object to exceed a given value. This strategy is still difficult to apply as such with concrete 3d printing process due to the discontinuity of the tool path,

which is a practical requirement for concrete printing when using a bi-component material. The flow is indeed hard to stop for self-compacting mortar or concrete since gravity can impact significantly.

- other additive manufacturing technologies such as Selective Layer Sintering (SLS), Stereolithography (STL) or powder-bed printing for concrete (D-shape¹, ensure the fabrication of any object geometry without consideration of the cantilevers. Indeed the printing is made by selective transformation of matter in a bed or pool of material. If a cantilever were to be printed it would be supported by the material in the bed or pool that has not been transformed. These technologies have been developed for metallic material, glass, plastic or concrete. Soliquid², a French start-up uses this strategy to extrude concrete directly into a pool of gel. The concrete in suspension in the gel has time to set before before the ambient liquid is removed, revealing the entire structure.
- 3d printing of metal is usually performed by SLS. However for large-scale manufacturing, MX3D³ developed another technology using a 6-axis robotic arms equipped with welding systems to build a large-scale stainless steel bridge in the Netherlands.
- Research on clay printing of cantilever is also ongoing [16], and is subject to the similar constraints as the printing of cementitious material. Hence most of the design space exploration in this paper can be applied to this material.

1.3. Masonry and mortar 3d printing

Masonry is one of the first construction system ever invented while 3d printing figures amongst the latest de-

veloped. Yet, their similarities in terms of material behaviour and layering process are apparent, which leads us to a deeper study of the comparison at different scales illustrated in Fig. 2: the brick, the layer and the final object geometry.

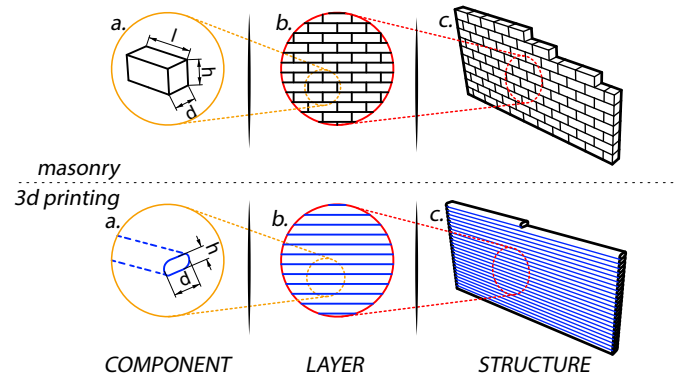


Figure 2: Masonry wall vs. 3d printed wall at the three different scales

1.3.1. The bricks and the extrusion

A masonry structure is made of discrete elements - the bricks - with 3 dimensions (height h , length l and width d) connected together using mortar which ensures stability after it has set. A 3d printed object is made of a continuous layer defined by 2 dimensions (its height h and width d). The bonding between layers is provided by the extruded material itself. Therefore the evolution of the concrete properties with time is key in the whole printing process.

Reiter illustrated in [17] the relation between the yield stress τ of the material and the time since the extrusion with the possible failure modes occurring during the process. In practice, the challenges with the material go beyond the simple stability of the built object. In [18], Lim *et al.* identified four material requirements: pumpability, printability, buildability, and open-time. These requirements combined with robotic freedom and process parameters control lead to the development of two asymptotic printing strategies: the "infinite brick extrusion" and the layer pressing strategy.

The consequences of these strategies on the extruded

¹The Radiolaria Pavilion — <https://dshape.wordpress.com>

²<http://soliqoid.io>

³<https://mx3d.com>

material properties are described by Roussel in [19] with in the first case a high initial yield stress layer (around 1000 Pa) which takes the form of the nozzle. And in the second case, a layer with a low initial yield stress (around 100 Pa) whose section can vary by playing with the printing parameters.

1.3.2. The layering sequence and final object

The second scale to consider is the layers (Fig. 2.b). In both masonry and 3d printing, the layers are mainly horizontal, and of similar height.

Masonry structures are assembled by stacking hundreds or thousands of components, either manually or robotically [20]. Their construction is characterised by the repetition of numerous assembly sequences, with a risk of error propagation. 3d printing is also characterised by a high number of simple steps, namely the deposition of the lace. The automation of the process and the precision of gantry or industrial robot reduces the error propagation. The work of Gramazio and Kohler [21] gives an insight on how digital manufacturing helps to broaden the design space of masonry structures and by extension how it can help define the design space of 3d printing.

A goal of 3d printing is to be able to let the robot work completely autonomously - without or with very little human assistance - and continuously, from the start to the end of the structure fabrication. Continuous printing is a necessity to ensure a good bonding between consecutive layers and mitigate potential cold joints. In addition, stopping and restarting the printing head repeatedly is a technological challenge that has not yet been solved or published for technology using accelerators due to the high fluidity of the fresh mix (at low flow rate, gravity is forcing the material down) and the risk of plugging the system after an extended stop. Although stop and start procedures are possible in some extent with infinite extrusion technology, each stop/start procedure involves a risk of inaccuracy due to settlements of the fresh structure.

Therefore in this paper, we assume the continuity of the layer to be a printing requirement. In unreinforced masonry, since the bonding comes with the mortar, which is applied in the same time as the upper layer, an unfinished wall can be left as is for hours or days without it changing its final mechanical behaviour.

For 3d printing of cementitious materials, two types of robots are mainly used:

- 3 or 4-axis Cartesian robots whose movements are translations in X, Y and Z directions and in some cases a full rotation of the nozzle (4th axis). In practice, the printing head is connected to a gantry bridge, a very stiff structure ensuring high precision of the nozzle position even at high speeds. If curve printing is possible with this kind of mechanism [22], it is mostly used for so-called "2.5D printing", each layer being printed in a horizontal plane.
- 6-axis robot articulated arms with 6 rotating joints giving the nozzle 3 degrees of freedom of translation and 3 degrees of freedom of rotation. The extrusion can be done at any point in space, in any direction (within the workspace of the robot).

6-axis mechanisms offer more freedom of movement and orientation during the printing than 3 or 4-axis mechanisms. But this is done at the expense of computational complexity of the toolpath generation (defined as the trajectory along with information on speed, acceleration, etc.) and calibration, due to the large number of axes and the non-linearities of the rotations.

1.3.3. Construction vs final structure

Finally, a similarity between masonry and 3d printing that might be the most significant is that due to its constitutive material, the behaviour of a 3d printed structure is different between construction and final state. Both elements work well in compression but poorly in tension. The only structural elements which do not involve any bending

or tensile force both during the construction and in their final configuration are a vertical walls and columns (see Fig. 2.c).

To increase the design space of geometry that can be built in masonry, temporary supports can be used during the construction so that only the final mechanical behaviour of the structure is taken into account during conception. For concrete printing, Tay *et al.* [23] proposed a solution to print the support simultaneously with the structure and play with the printing parameters so that the temporary parts can easily be removed in the end.

Research in shell and spatial structures has led to efficient form-finding tools for thin shells in concrete or masonry [24] allowing for final structures to work only in compression providing an efficient use of the material. However, those structures need a full temporary scaffold, which is as expensive and time-consuming as the structure is complex.

Solutions to build cantilever structures in unreinforced masonry without temporary supports have been developed in the past to overcome:

- the lack of available material for the scaffold, especially wood in dry areas;
- the heavy costs of such a scaffold (30% to 60% of the structure cost [25], for concrete casting);
- the technical difficulty to build a scaffold (as it was the case during the construction of the 45m diameter dome of Florence cathedral built more than 50 metres above the ground);

Those strategies made a compromise between the behaviour of the structure during the construction and its mechanical efficiency in its final state. The main strategies, detailed and illustrated by Auguste Choisy in [26] will be discussed later in this paper.

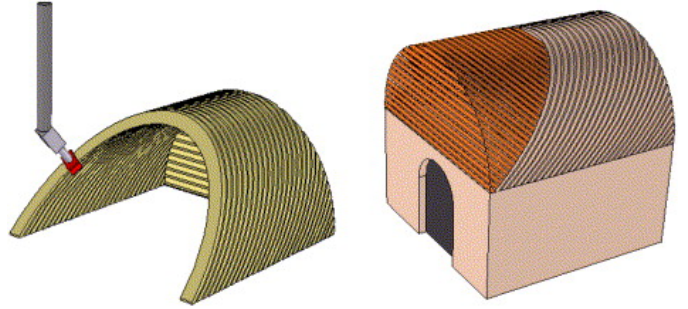


Figure 3: Scheme for construction of a Nubian vault by Contour Crafting by Khoshnevis published in [28]

1.3.4. Problem statement

The comparison between 3d printing processes and masonry structures has naturally come up in the first proposals for printed large-scale structures. In his seminal article on 3d printing of cementitious material [27], Pegna refers indeed to 3d printing as "a new approach to masonry". In [28], Khoshnevis mentions the possibility to use 3d printing for the construction of barrel vaults without external supports (see Fig. 3).

The goal of this paper is to go beyond the simple comparison between two additive manufacturing processes, and to focus on specific strategies used in masonry to build cantilevered structures and how to apply them to mortar or clay 3d printing to broaden the design space of printable geometries. The first section provides an introduction on the topic of cantilever printing through an analogy between masonry and 3d printing. The second section proposes a classification of possible strategies based on initial material stress, support complexity and brickworks continuity. This classification is applied to different typologies of masonry structures in the third section. In the fourth section, a parallel is made with 3d printing and a design framework for building cantilever shapes is proposed, taking into account the material formulation, the control of the process and the robot used. Some strategies found in historical structures are proposed as a proof of concept.

2. Cantilever structures in masonry

A classification of the fabrication process has been proposed by Duballet *et al.* [29] in order to help actors in the field of 3d printing to explore this new design space efficiently. It is based on the environment, the scale of the printed object, the need for supports, etc. Following the same methodology, this part is an attempt at classifying masonry structures that present cantilevers, with criteria describing the brick stress in its initial state, the fabrication process and the supports in use. Then a state of the art of strategies to build cantilever structures in masonry is used as examples of application of the classification. A parallel is made between the criteria proposed by the authors for masonry structures and the parameters at stake in mortar 3d printing processes.

2.1. Use of support

The first criteria regarding support of the structure has already been introduced in Duballet's classification. It was divided in 4 categories:

- no support
- printed supports left in place or removed afterwards
- external supports left in place or removed afterwards

The present classification concerns masonry structures and thus refers only to categories s^0 (no supports) and s^4 (external supports removed afterwards). The asterisk in the following criteria shows subcategories of the existing criteria s^4 . They are illustrated on Fig. 4:

- s^{*1} **punctual supports**. This refers to structures built using temporary columns or cables to maintain the bricks in place until completion of the construction. Examples can be found in arches or vault assembly using cables to keep funicularity in the temporary structure [30].

- s^{*2} **boundary linear support**, such as lintel for an opening in a structure or to the gable wall supporting the starting edge in the construction of Nubian vaults.
- s^{*3} **internal linear supports**. Used in Gothic architecture to build internal ribs, supporting later the construction of the actual vault.
- s^{*4} **fully supported structure**. Refers to structures built onto a scaffold. The structure gains its final mechanical behaviour after the complete removal of the scaffold ([31],[32] show the design process of the Armadillo Vault by Block *et al.*, a fully funicular vault in unreinforced masonry but which requires a full scaffold for the set up of the voussoirs). This criteria is out of the scope of this paper by definition.

2.2. Initial brick stress state

This criteria classifies the assembly process based on the initial stress state of the brick, just after it is set in the structure. We look here at the brick element positioned with or without mortar, before completion of a full layer that would create a compression ring for example, changing the stress inside the element. The specification on the time dependence of the criteria comes from the assumption that most masonry vaults are designed to be funicular. In mortar 3d printing, the initial state involves the material with its weakest properties, this step is thus decisive for the success of the fabrication process.

- f^0 **shear stress**. The element is set onto the previous layer at a certain angle using friction to stay in place.
- f^1 **bending and shear stresses**. The element is set with an angle and an offset from the previous layer creating a local cantilever.
- f^2 **bending moment**. The element is set on the previous layer horizontally with an offset, creating a local cantilever.

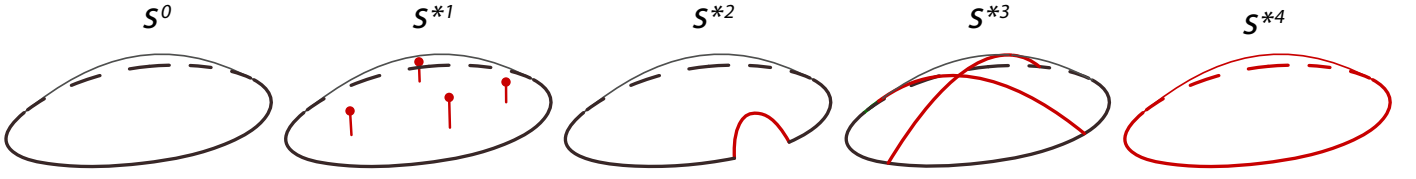


Figure 4: Illustration of the different types of supports

Fig. 5 illustrates criteria f for different layer configurations.

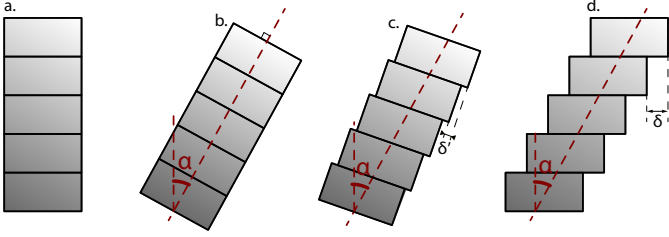


Figure 5: a) vertical wall, b) f^0 shear stress coming for the layer inclination of angle α , c) f^1 combination of bending and shear in the material, d) f^0 bending moment coming from the local cantilever δ

By using Mohr-Coulomb theory (Eq. 1) as it is usually the case in masonry [33], a simple comparison between the initial stress in the layer in the different configurations can be made.

$$\tau < c + \sigma \tan(\phi) \quad (1)$$

Let's consider the top layer on Fig. 5, inclined of an angle α , subject to its self weight only $F = \rho gh dl$ and we note $A = dl$ the linear contact with the previous layer. We can define the normal and shear stresses of the material at the interface between previous layer:

$$\begin{aligned} \tau &= \frac{F}{A} \sin(\alpha) \\ \sigma &= \frac{F}{A} \cos(\alpha) \end{aligned} \quad (2)$$

We introduce the non dimensional parameter $\beta = \frac{c}{\rho gh}$, and after a calculation detailed in Appendix A, we find that:

$$\alpha_{max} = \begin{cases} \phi + \arcsin(\beta \cos(\phi)) & \text{if } 0 < \beta \leq 1 \\ \frac{\pi}{2} & \text{if } \beta > 1 \end{cases} \quad (3)$$

In the assumption of no cohesion ($\beta = 0$), one finds that the critical angle is simply $\alpha_{max} = \phi$ and does not depend on the blocks scale. This criterion is often used in preliminary design stages for masonry structures. The case $\beta > 1$, where layers can be printed horizontally ($\alpha = \frac{\pi}{2}$) is illustrated in section 4.6 of the paper with the fabrication of a horizontal cylinder without any supports.

In the case of cantilever obtained with corbels (Fig. 5.b), we can apply the analysis above to the offset part only. This comes down to analyse a layer of thickness δ and inclination $\alpha = \frac{\pi}{2}$. Equation (3) tells us that it is possible only if $\beta_{f^2} \geq 1$. The relation between the offset δ , the thickness of the layer h and the global inclination of the wall is given by the relation $\tan(\alpha) = \frac{\delta}{h}$. So we simply find:

$$\frac{c_{f^2}}{\rho gh} \geq \tan(\alpha) \quad (4)$$

For a material with a friction angle $\phi = 0$, we obtain for a wall with inclined layers:

$$\frac{c_{f^0}}{\rho gh} \geq \sin(\alpha) \quad (5)$$

The graph on Fig. 6 shows that when the criteria is f^0 the critical angle α is always larger than for f^2 criterion. The ratio is one for $\alpha = 0$, which corresponds to a straight wall. This simple analysis gives a first advantage in inclining the layers instead of creating local cantilevers.

The criterion f on brick stress and the geometry at component scale are closely related. Fig. 5.b and .d, show layers inclined at a constant angle. The section of all layers are rectangles rotated of an angle α . For many other geometries, this angle does not remain constant during the fabrication, as shown for example on Fig. 7 for a curved object. In that case, the object can not be divided in

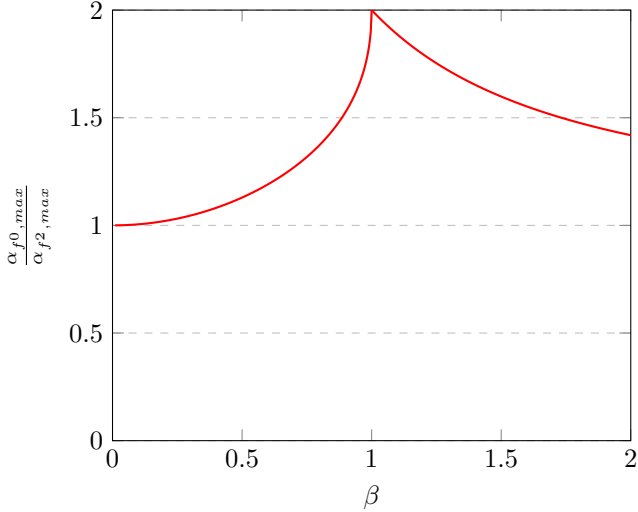


Figure 6: Comparison between f^0 and f^2 critical angle

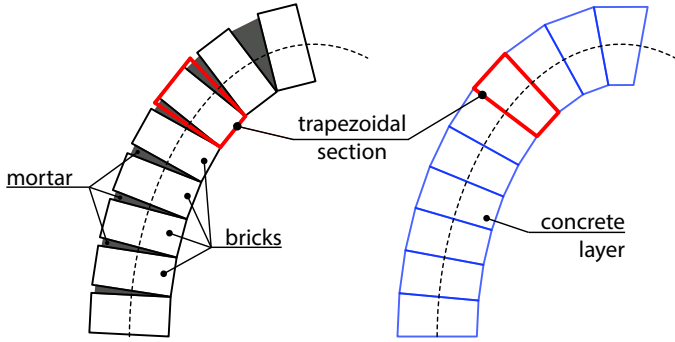


Figure 7: *left*: masonry curved wall, *right*: 3d printed curved wall

rectangles, instead the laces have a trapezoidal section. In masonry, this is achieved by either using the mortar to correctly orient each brick, or by cutting the brick in trapezoidal shapes beforehand. For 3d printing, it implies that the process has the capacity to shape the layer when it is extruded. The combination of a f^0 or f^1 criteria with curved geometry (α not constant) leads automatically to a variation of the shape of the section and thus to necessary additional features on the printing technology used.

2.3. Layers continuity

Masonry structures are built with discrete elements. They can be assembled using complex brickworks for aesthetic or mechanical purposes. The present criteria serves at describing if the structure can be built following a linear setting of the bricks, or not. The continuity is influenced

by the topology of the object. It can also come from a design choice for aesthetic or mechanical purposes, or fabrication constraints.

- **c^0 continuous layer.** This strategy used in most cases consists in assembling a layer by setting one brick after the other continuously, and stacking layers onto layers until completion of the structure.
- **c^1 piecewise continuous.** It refers to structures built by separate blocks. Each block taken independently is continuous c^0 . This happened in Persian vaults built on squinches for example. Each squinch is elevated separately from the others until they are all connected to form the final structure.
- **c^2 discrete assembly.** Refers to complex brickworks such as the herringbone used for the construction of the dome of Florence cathedral by Brunelleschi. The layers do not form a continuous alignment of bricks, preventing in this case the creation of slipping plane that would lead to an early breakdown of the structure during construction. As stated in the introduction, the scope of this article is focused on continuously printed layers. Hence, in this case, the analogy between brickworks and concrete printing does not hold. The criteria is still mentioned as those limitations may disappear in a foreseeable future.

The three criteria are illustrated in Fig. 8 where a same wall is built with different brickworks, impacting the assembly process of the masonry structure.

3. State of the art of cantilevered structures in masonry

To illustrate this classification, we apply it directly to existing masonry structures. The following part is a recollection of main strategies used to built vaults or domes without temporary support (or as minimum as possible).

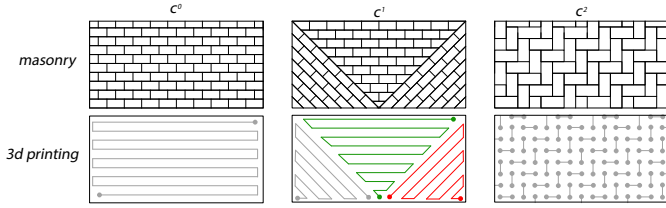


Figure 8: Illustration of the layers continuity by comparison of masonry brickworks and equivalent 3d printing path with *left*: continuous brickwork, *middle*: patched masonry and *right*: discontinuous brickwork. The dots mark the discontinuities and the stopping and restarting of the system.

3.1. Corbels - $s^0 f^2 c^0$

The simplest way to build cantilever in masonry is to use the technique of corbelling. In 2 or 3 dimensions, it consists in creating a local cantilever of each horizontal layer onto the previous one, generating thus the global cantilever. This strategy has been used in stone construction in Ancient Greece (*Treasury of Atreus* in Mycenae showed in Fig. 9), as well as in rural areas of France (bories) and Italy (trulli [34]) to quickly build protective shacks the easiest way possible with available material. It is described by Cowan in [35] and Choisy in [26], stating that such structures have been discovered in Egypt from about 2900 B. C.

The stability of the temporary structure is ensured if there is no opening of the bed joints during construction. This can be achieved by adding counterweight on top of the location where joints are more likely to open. This strategy creates bending in the bricks. The other solution is to stack the brick in a way that the centre of mass of the overall section, when projected vertically onto the ground, is contained within the footprint of the first layer. This approach has serious limitations when trying to minimise material quantity and maximise its efficiency:

- in two dimension the relation between the span S and the global height H of the structure given by Hall in [36], shows that:

$$\frac{H}{h} \propto \exp \frac{2S}{d} \quad (6)$$

where d and h are respectively the brick width and height according to previous notation. This equation shows that the height increases exponentially with the span, and thus limits the strategy to small structures.

- since the width of the bricks is determined by construction constraints, the final thickness of the vault is bigger than necessary, implying an inefficient use of material. In addition, due to construction process, the main thrust lines are not perpendicular to the voussoirs interfaces.

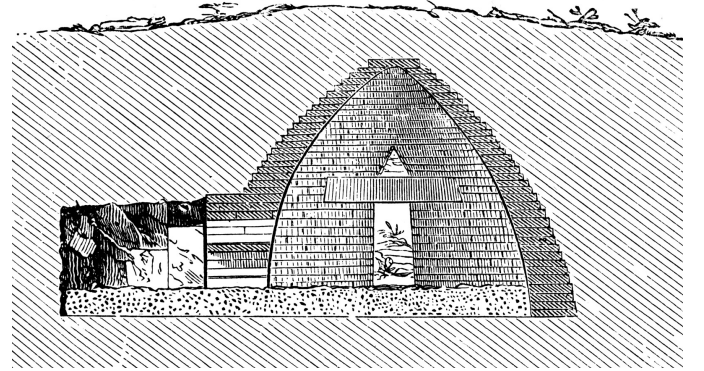


Figure 9: Treasury of Atreus, Mycenae, Greece. Source: Wilhelm Lübke, Max Semrau: Plan of Art History. Paul Neff Verlag, Esslingen, 14th edition 1908

3.2. Nubian Vault - $s^2 f^1 c^0$

Barrel vaults around 3300 years old have been found in Egypt in the region of Gournah. Those structures built by the Nubians are composed of inclined arches laying onto each other. The construction starts by disposing the bricks on a gable wall until the first arch is set. Then a horizontal translation of this arch creates the vault. Fig. 10 shows the basic typology of the structure, with the gable wall and the inclined arches. From a structural point of view, the construction process can be divided into three phases.

- First the deposition of the brick is made on an inclined bed joint, meaning the stability is ensured by the mortar holding the brick in place temporarily.

- Once all the brick of an arch have been installed, a thrust line appear in the arch putting the bricks in compression and allowing them to withstand the loads from the future arches.
- Finally, when an arch is far enough from the construction area, it is not impacted anymore by the new added layers. The principal stress directions in this area are independent from the inclination of the arches.

We notice here that if the angle of inclination of the arches is constant, even with a f^1 criteria (shear and bending), the whole structure can be built with bricks of constant rectangular section. This refers to the final remark in the part describing the brick initial stress state f .

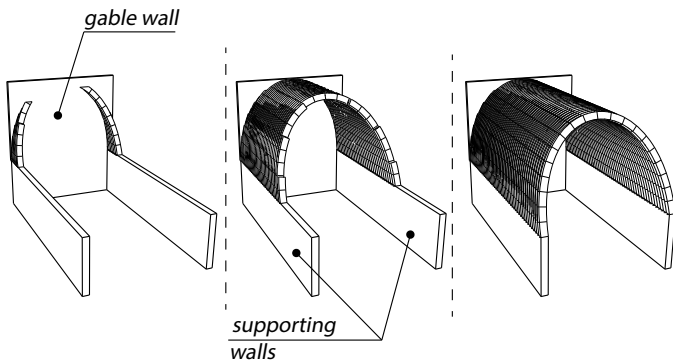


Figure 10: Construction of a Nubian vault

3.3. Dome with inclined layers - $s^0 f^0 c^0$

In order to build a dome without local cantilever, what Cowan named a "true dome" in [35], the layers have to be inclined so that their upper and lower faces are normal to the thrust in the structure. This prevent any sliding along the interface, maximise the contact area between layers and maximise the utilization of the material. Gaspard Monge theorised stereotomy for such structures following geometric principles as reported by Sakarovitch in [37] under the name "constructive geometry". In the case of brick masonry, the elements are positioned and adjusted correctly by deforming the layer of mortar in between. As illustrated in Fig. 7, the section of the layer is trapezoidal.

The stability of the temporary structure comes from the formation of compression rings locking the bricks in position (see Fig. 11) without creating bending moment in the material or opening of the joint.

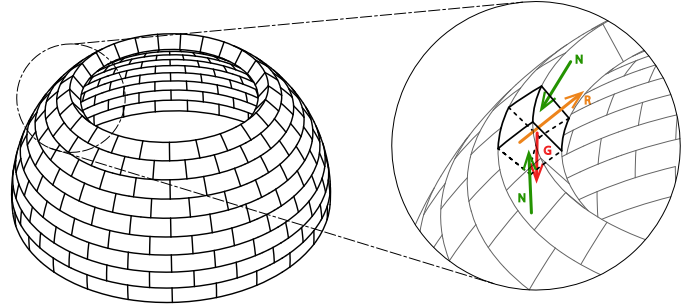


Figure 11: Masonry dome on inclined layers

This strategy presents also some limitations:

- when the radius of the dome is too high, the curvature of the layer is low, and so is the geometric stiffness. The compressive stress holding the ring together is then more likely to reach values that can cause either a plastic failure of the material, or a local buckling of the layer leading to a global collapse of the object.
- in a "true dome", the inclination of the layers increases continuously to reach a fully vertical position at the apex. This is hardly possible when building with no temporary support (whether in masonry or 3d printing). Given that α_{max} is the maximum inclination angle of a layer given by eq. 3, a dome could be built in a classic way until α_{max} is reached. Then the layers inclination remains constant, giving to the dome a conical shape in its upper part (see Fig. 12). Choisy even suggests this constraint to be the main reason behind Persian and Byzantine noticeable architecture of domes [26]. This strategy recalls the level-set method of Cacace *et al.* in [12] for optimisation of supports in FDM process, but with the constraints applied to the final structure instead of the temporary supports.

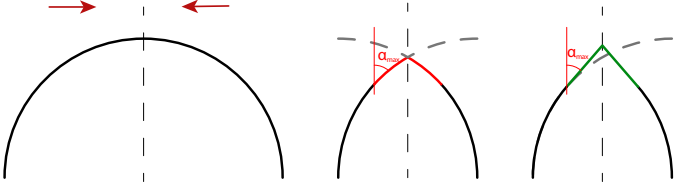


Figure 12: Modification of a dome shape based on the maximum admissible angle α_{max} defined in eq.A.7

3.4. Catalan vault - $s^0 f^2 c^0$

Catalan vaulting techniques as for the previous true domes, use double curvature in order to cover large area without needing any support. The tiles are positioned on their edges using fast setting plaster. Their lightness allows the structure to withstand the bending force created by the addition of a tile. as soon as a layer is built, compression is predominant. The first layer of tiles is also used to support the second and usually third one, bringing bigger thickness to the structure shell and increasing the rigidity and decreasing the risk of collapse by buckling. the technique of the Catalan vault has been perfected by Guastavino and described in [38]. This technique allows to build funicular vaults and domes and has recently made a come back with the apparition of new computational tools for form-finding of masonry structures [39].

3.5. Persian vault - $s^0 f^0 c^1$

The Persians were prone to build a dome without support by inclining the layers and creating compression rings. However, the actual buildings did not always present a circular boundary to start the dome. Most vaults were supported either on four walls or on four columns. Hence the development of pendentives and squinches around the years 250 AD [40]. As illustrated in Fig. 13, those peculiar brickworks are stable on their on, and they allow to go from a given boundary condition to a circular layer from which it is easy to build a simple dome. They act by locally modifying the curvature of the surface to reduce the bending moment coming from the cantilever by coupling it to the normal stresses. This is of course not an exhaustive

description of Persian architecture but merely a mention of their contribution to supportless fabrication of domes with squinches.

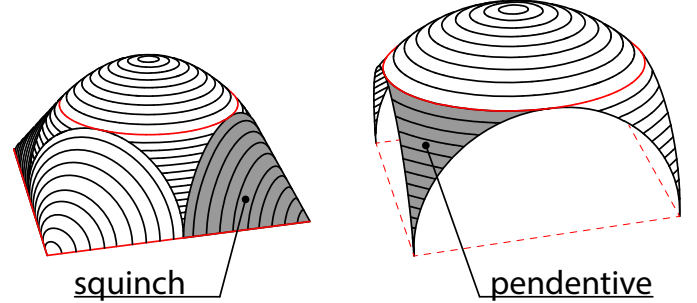


Figure 13: Squinches and pendentives with discontinuous layering

These brickworks can also be used when the base of the dome is circular but the diameter is too high to ensure the stability of the compression rings as we discussed earlier. In this case the squinches artificially bring more curvature and thus more stability at the expense of using more material.

3.6. Gothic vault - $s^*3 f^0 c^1$

For construction of Gothic cross-vaults, or rib vaults, Fitchen described in [41] a strategy to build the vault with a simple stone-weight rope device (see Fig. 14). The diagonals are built first using linear centering. Then for the construction of the actual vault, each additional block is temporary stabilised by the rope device which applies a punctual force tangent to the surface of the vault, keeping the structure in compression.

3.7. Interlocking systems - $s^*1 f^1 c^2$

Interlocking systems in masonry implies that each block is geometrically prevented from moving by its adjacent blocks. The most notorious example of such system is the Abeille Vault developed in the 17th century [42] [43]. Since a block is stabilised as soon as the next one is set, this kind of structure can be built using temporary supports only for the elements on the edges. Those structures

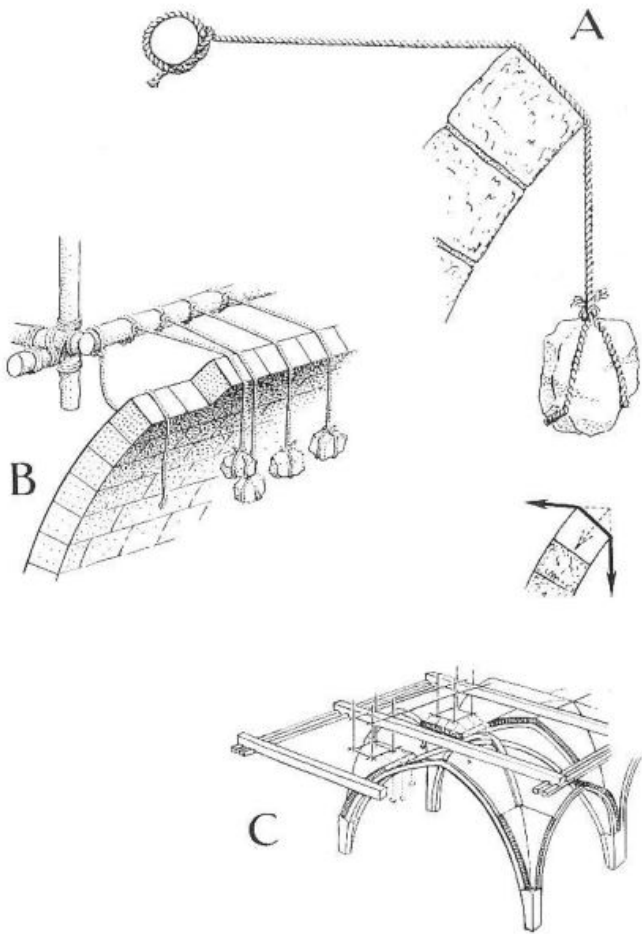


Figure 14: The stone-weighted rope device for erecting Gothic vaults (John Fitchen, *The Construction of Gothic Cathedrals*, 1961, fig. 69, p.182)

requires precise and time-consuming stone cutting beforehand or modern fabrication technology as it was the case for the vault of Fig. 15 where the blocks were 3d printed and intended to be assembled robotically [44].

Special discontinuous brickworks can also be used to ensure stability of the structure at the scale of the layer. For instance, Brunelleschi built the dome of Florence cathedral in the 15th century, in masonry, without support, using a herringbone brickwork [45] that alternates vertical and horizontal elements avoiding thus the creation of sliding planes. This category of brickworks involves discontinuous elements (c^2) and as mentioned earlier, can not be yet implemented for 3d printing processes.

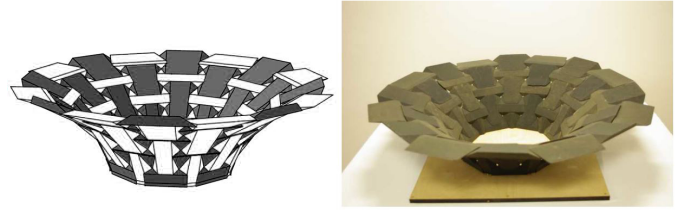


Figure 15: Vault built with interlocking bricks by Vianney Loing

3.8. First results

The following table 1 regroups all previously mentioned masonry structures with their respective criteria for support, brick initial stress state and layer continuity. Fig. 16 categorises the different typologies of structures aforementioned and examples of 3d printed objects based on their behaviour at different scales: the scale of the section with the initial stress state, and the scale of the layer with the existence or not of a structural sub-system. This sub-system can be:

1. a compression ring usually present in circular domes.
2. an arch in compression, seen in Gothic vaults built on ribs or barrel vaults such as Nubian vault. Note that when successive layers are connected, the structure behaves as a shell and not as a series of consecutive arches, improving its mechanical performance.
3. a layer with tensile stress. Although masonry structure and concrete are not envisioned to withstand tensile stresses, their yield stress in traction is not zero even in a fresh state and it is possible to play with this small leverage to create cantilever.

The table also contains an example of a 3d printed vault fabricated on a full support, to illustrate what has been done so far.

Masonry structure typology	Support	Brick initial stress state	Layer continuity
Corbels	s^0	f^2	c^0
Nubian vault	s^{*2}	f^1	c^0
Dome with inclined layers	s^0	f^0	c^0
Interlocking systems	s^{*1}	f^1	c^2
Catalan vault	s^0	f^2	c^0
Persian vault	s^0	f^0	c^1
Gothic vault	s^{*3}	f^0	c^1

Table 1: Summary of masonry vaults typologies and their parameters

We can now put in relation 3d printing process of cementitious material and our new classification for masonry structures built with minimum temporary supports. We have already discussed in part 2.2 the relation between the brick initial stress state criteria f and the capacity to control the extruded layer geometry. These two aspects are also correlated to the material properties. A lace printed with a material with high initial yield stress and viscosity, (case of the "Extruded lace shaping"), takes the shape of the nozzle. It is the best choice when the layer has to withstand high initial stresses, such as bending moment caused by a local cantilever (f^1 : *bending and shear*, or f^2 : *bending moment*). Extrusion with very low initial yield stress and viscosity ("Orienting lace pressing"), results in a layer unable to withstand much more than a shear stress (f^0 : *shear stress*) when coming out of the nozzle, but offers the possibility to modify its geometry. This relation between material properties, initial stress state and layer geometry control is illustrated in Fig. 17.

From a technology point of view, we described robotic complexity in our case to be proportional to the number of axis of the robot. The more axis, the more freedom

in the geometry, but the more difficult it is to calibrate the robot (or working area) and generate a toolpath. A Cartesian robot is not able to print an object where the layers orientation is changing as in Fig. 7. In that case, cantilevers can only be created using corbels (f^2 criteria) with a high initial yield stress material.

Layer geometry control can be provided by 6 axis robot whose orientation can be set for each target. The support parameter s , also has an impact on the choice of the robot. Any support brought in the process needs to be calibrated before the works start. By adding supports, we thus increase the calibration works whose difficulty increases with the number of axis.

The same reasoning can be made to relate robotic complexity with layers continuity c . Discontinuous toolpaths of a continuous surface are more likely to involve changes in orientation of the layers (see Fig. 2) and additional supports (see example on Gothic vaults). Thus discontinuous layers would naturally lead to higher robotic complexity.

4. Application to 3d printing of cantilevered structures

In practice, the design process leading to the fabrication of 3d printed object in cementitious material can be divided in different steps which are increasingly complex and process-dependent:

- defining the structure geometry and its boundary conditions;
- defining the layers by slicing the object and thus generating the robot trajectory;
- setting the printing parameters based on the layers section, the material and the printing equipment.

This process can be iterative, modifying the slicing direction or the geometry until the complete toolpath can be generated. It is summarised in table 2.

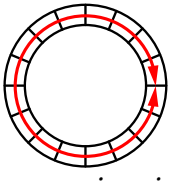
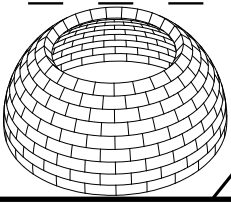
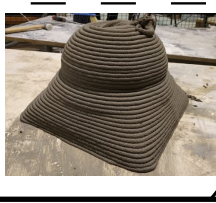

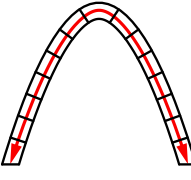

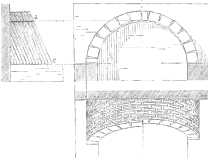
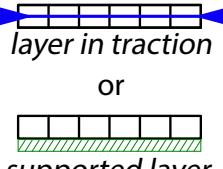



		Initial stress state		
		f^0	f^1	f^2
Structural sub-system	 compression ring	$f^0 \quad s^0 \quad c^0$  a	$f^1 \quad s^0 \quad c^0$  b	$f^2 \quad s^0 \quad c^0$  c
	 arch	$f^0 \quad s^3 \quad c^1$  d	$f^1 \quad s^2 \quad c^0$  e	no known example
	 layer in traction or supported layer	$f^0 \quad s^0 \quad c^1$  f	$f^1 \quad s^4 \quad c^0$  g	$f^2 \quad s^0 \quad c^0$  h

Figure 16: **a.** True dome with inclined layers, **b.** 3d printed dome by corbelling horizontal layers. The local cantilever of the section leads to a gradual inclination of the layers, **c.** Borie, traditional habitat for shepherd in South East of France during transhumance. The borie is made of corbelled stones, **d.** Gothic vault of Saint-Séverin church in Paris, France. The ribs are built first using linear formworks then the parts of the vault is constructed, each layer creating an arch between the existing ribs. Credit photo: Roman Bonnefoy, **e.** Nubian vault drawn by Auguste Choisy showing inclined brick layers forming successive arches, **f.** 3d printed arch built without temporary supports. The layers are inclined to avoid local cantilevers and to limit the longitudinal tensile stresses, **g.** Assembled 3d printed concrete vault where each piece is extruded on a full support providing the double-curvedness. Image from [46] by Borg Costanzi et al., **h.** 3d printed castle by Andrey Rudenko showing corbelled layers to create the windows and doorway.

4.1. Boundary conditions and global geometry

As we saw with the examples of masonry structures built without or with little temporary support, the range of geometries that can be achieved is wide. In table 2 the authors propose primitive shapes based on boundary conditions (namely the supports of the structure) and a selected profile. This profile is either translated, rotated or untouched to form respectively a barrel vault, a dome (faceted or not) or a simple arch. Historically, vault sec-

tions (the so-called "profile") are regular geometries composed of circular arcs. This way, vaults and domes could be described physically by the only tools at the disposal of the mason (Mason's thread, etc.). Fig. 18 shows examples of arches that can be drawn using only circles of different radius.

This geometric limitation disappears when using a robot thanks to its absolute precision in space. Therefore, designers should target geometries that make the best of

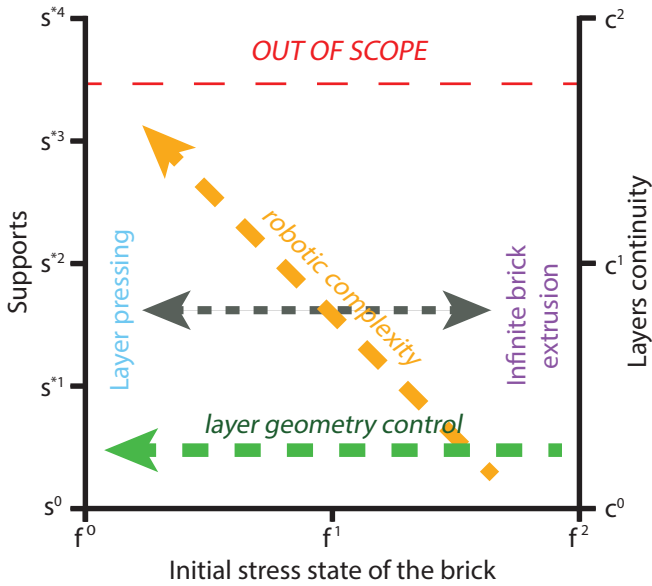


Figure 17: Relation between masonry parameters s , f and c and mortar 3d printing set-up

the material. In the present case, the targeted geometry to be 3d printed must be as close as possible to the funicular of the self-weight of the structure and potential external loads specific to the object function, so that the final object is fully in compression.

4.2. Generation of the robot trajectory

This part describes the process of generating a toolpath trajectory describing the movements of the robot from an object geometry. We propose again an approach with two asymptotic strategies that can be related to the material and the technology used.

- The more common strategy is to slice the geometry horizontally using a constant vertical offset (see Fig. 19 left). The resulting curves are divided into targets whose orientation is always a horizontal plane. The toolpath generated can be written in Gcode and the object can be printed by a 3-axis Cartesian robot. If the object presents cantilever parts, they can only be

achieved by corbelling layers (f^2), requiring a material with a high initial yield stress. This is the strategy used when printing with plastic (PLA, ABS, etc.) and using a standard slicer like Cura for example.

- The opposite strategy aims at creating only shear stress in the material (f^0), it was described by Goselin *et al.* in [5] as "Tangential Continuity Method". The slicing must generate curves of constant distance between them. For a circular geometry, this comes down to a radial slicing as illustrated on Fig. 19 middle. For more complex geometries, this layering can be achieved using the algorithm developed by Adiels *et al.* and detailed in [47]. It proposes a solution for bricklaying with a constant geodesic height using orthogonal curves to geodesic lines on the surface, which perfectly applies to mortar 3d printing as well. In [48], geodesic lines are directly used as robotic path, leading to thickness variations in the layers but the targets are always perpendicular to the object surface. The targets orientations are obtained from a Darboux frame at each position, made from the outgoing normal to the surface of the object, the tangent to the layer curve and the cross-product of the two (Fig. 20). The extrusion is made in the direction of the latter vector. In this case, a 6-axis robot is necessary to reach all positions of the toolpath. From a material point of view, the initial brick state in the layer is optimised by avoiding any local cantilever. Fig. 25 shows an example of a Nubian vault 3d printed using this strategy. The layers are inclined with a constant angle but the robot head remains tangent to the surface to maximise the contact surface between layers and reduce local offset between layers. A video of the printing of this vault is available [49], and it gives an understanding of the robotic movement as well as the deformation of the sub-layers when the material is pressed during the extrusion.

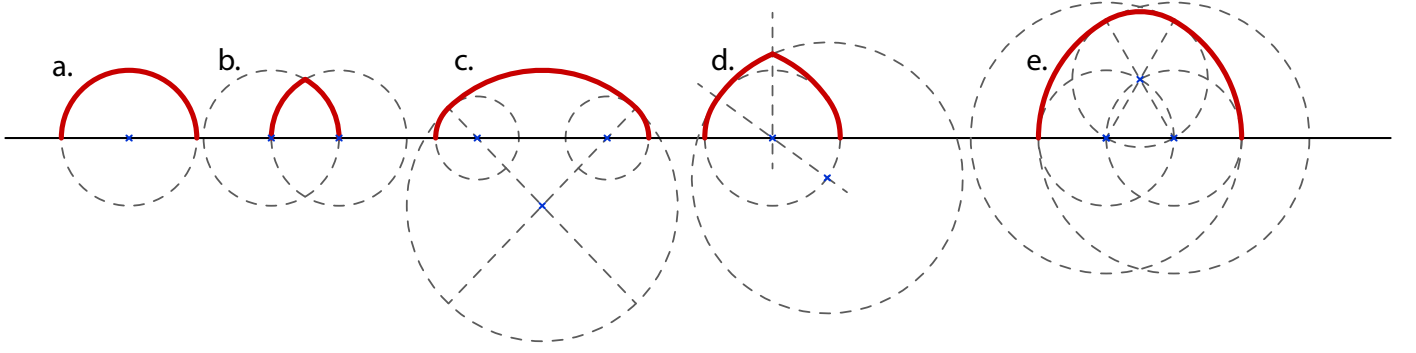


Figure 18: Examples of profiles composed of arcs of different radius. Note the tangential continuity ensured by the alignment of the circles centres and the transition points on the circles

In practice, it is not always easy to stay tangent to the surface due to possible obstruction of the robot or to the material properties preventing printing above a maximum angle for example. In that case the second strategy can not be applied directly, and other slicing solution might be used locally, like constant angle slicing (Fig. 19 right).

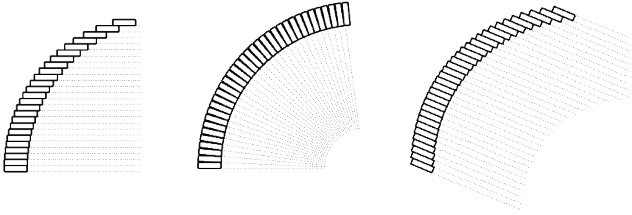


Figure 19: Slicing strategies. a. horizontal slicing, b. constant layer thickness, c. constant angle slicing

4.3. Printing set-up and parameters control

The last step in generating a toolpath is the setting of print parameters: the robot speed V_r and the concrete flow rate (volumic) Q_c . They are related to the layer's cross section $A = h \cdot d$ by the mass conservation equation (7). The robot speed evidently influences the inter-layer time. There are however practical limitations in the variations of robots speed to accommodate inter-layer time, and which might make a path unfeasible.

$$Q = V_r \cdot h \cdot d \quad (7)$$

In practice, the volume flow rate is limited by the capacity of the pump, or by the maximal speed of the robot,

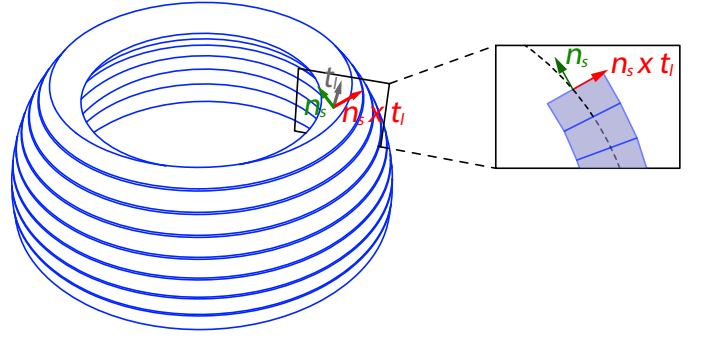


Figure 20: Darboux frame from the object surface and the layer direction

the second case being unlikely for large 6 axes robots. Due to the mass conservation, this means that the maximal and minimal speed of the robot are bounded. This bound does not depend on material properties, but rather on the printing set-up and can precisely be determined.

$$V^- < V < V^+ \quad (8)$$

We shall look now at the compatibility between a tool-path and the rheological properties of the mortar. Assuming for simplification that the printing path is a collection of curves Γ_i of length l_i , for which the robot speed is constant V_i , the total printing time is simply defined by equation (9).

$$T = \sum_i \frac{l_i}{V_i} = \sum_i \Delta t_i \quad (9)$$

The inter-layer time Δt_i between the layer i and the layer $i+1$ is l_i/V_i . It is constrained by the time window. In

order to maintain a seemingly constant time window, the speed must increase proportionally to the layer length. One expects thus for the speed to be maximal for the longest layer and minimal for the shortest one. This gives a geometrical limit that relates the ratio of curve length to the time window depending on rheological properties.

$$\frac{\max(l_i)}{\min(l_i)} < \frac{V^+ \Delta t^+}{V^- \Delta t^-} \quad (10)$$

The lower boundary of the time window depends on the structuration rate of the material and its capacity to withstand the weight of successive layers. Equation (11) gives an expression of this time window lower bound for a straight wall printed at a constant speed and with a material having a constant structuration rate A_{thix} [19].

$$\Delta t^- = \left(\frac{\rho g h}{\sqrt{3}} - \tau_0 \right) \frac{1}{A_{thix}} \quad (11)$$

The upper bound Δt^+ depends on both the material thixotropy [19], [50] and the printing environment. High thixotropy and dry environment are factors that can lead to the creation of so-called cold joints, which characterised weak cohesion at successive layers interface. This phenomenon is increased with time and its apparition is what defines Δt^+ . Roussel gives its analytical expression in [19]:

$$\Delta t^+ = \frac{\sqrt{\frac{(\rho g h)^2}{12} + \left(\frac{2\mu_p V_r}{h} \right)^2}}{A_{thix}} \quad (12)$$

where μ_p is the plastic viscosity. Although recent research [51] suggests that strength loss at the layers interface gets higher when the interfaces are exposed to fast surface drying, and that thixotropy is not responsible alone for poor cohesion between layers. The chemistry of most printable concretes is indeed often accelerated through the use of aluminate-based compounds. They can therefore reach temperatures, above which drying, even for a couple minutes, can not be neglected.

The boundaries of the time window might be difficult to assess precisely experimentally, while a satisfying time within the time window can be found. In practice, a user

might want to aim for a constant inter-layer time, which simplifies then the previous estimate.

$$\frac{\max(l_i)}{\min(l_i)} < \frac{V^+}{V^-} \quad (13)$$

By introducing parameter $\Omega = \frac{V^+ \min(l_i)}{V^- \max(l_i)}$, it comes directly that the object is printable by the set-up if $\Omega > 1$.

This kind of constraint can easily be implemented in a parametric CAD environment, like Dynamo or Grasshopper. It can be combined with equilibrium based methods [7], which lacks material information.

Fig. 21 is an illustration of implementation of this criteria on a dome. The range of the flow rate is taken between $20g.s^{-1}$ and $50g.s^{-1}$ which corresponds to the maximum and minimum capacity of the pump. The section of the layer is chosen equal to $120mm^2 - 20mm$ width and $6mm$ height. It comes directly from equation (7): $V^+ = 185mm.s^{-1}$ and $V^- = 74mm.s^{-1}$. Fig. 21.*left* shows the layers length gradually decreasing. Fig. 21.*middle* shows the printable part in blue and non-printable part in red obtained by calculating Ω for each layer by considering $\min(l_i)$ to be the length of the actual layer and $\max(l_i)$ being always the length of the first layer.

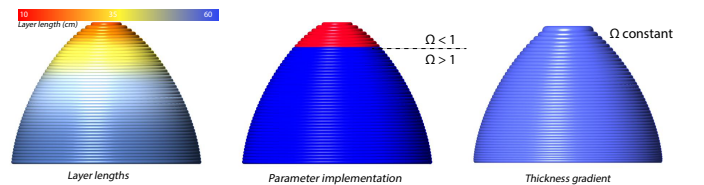


Figure 21: Geometric constraint verification in a CAD environment

To print the entire object without changing the overall geometry, one can either modify the section of the layers during the printing or change the inter-layer time. In the first case, one can see that by playing on the section, the speed limits V^- and V^+ can change without modifying the flow values. Increasing V^+ and decreasing V^- leads to a gradient of thickness in the layers with thin layers at the bottom and thicker layers at the top (see Fig. 21.*right*). This solves the problem from a cinematic point of view

but it changes the loading rate of the first layers and may increase the risk of instability of the structure.

In Fig. 22, the domes from Fig. 21 are actually printed. The one on the left has a constant layer thickness H . The inter-layer time Δt is constant until the flow rate Q reaches the minimal value achievable by the pump. The layers after that are printed at a constant flow rate and robot velocity V_r , decreasing thus the inter-layer time for each new layer. The dome on the right illustrates the capacity to modify the layer cross section on a single object. The linear increase in thickness H of the layer allows to keep a constant inter-layer time Δt while remaining within the working range of the equipment. It also helped to decrease the global printing time of the object from 15 minutes (for the one with constant thickness) to 10 minutes, for the same amount of material and same geometry. However, for the thicker layers (on the top part), a settlement can be observed, which lead to an error in the total height of the object.

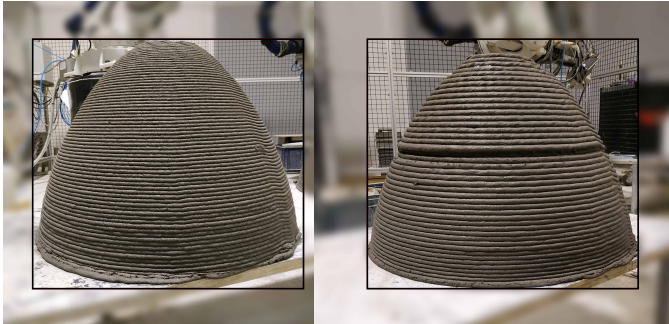


Figure 22: 3d printed domes with constant layer thickness on the left, and variable layer thickness on the right. The layer width B is the same in both cases and remain unchanged during the print.

The other strategy to ensure a good setting of the printing parameters, is to reintroduce the inter-layer time Δt in the calculation of Ω , following equation (10). This gives a new parameter $\Omega' = \frac{V^+ \Delta t^+ \min(l_i)}{V^- \Delta t^- \max(l_i)}$. Δt^- can be chosen so that $\Omega' > 1$ for all layers. In this case the material properties, namely the initial yield stress and structuration rate must be properly set to accommodate the smaller inter-layer time.

This final step in the generation of a toolpath gives information on the necessity to be adapting the parameters to the geometry of the object. By setting the geometry of the layers, the speed of the robot and the flow of concrete can vary during a print to ensure that equation 7, is verified. That way rheological constraint due to the setting of the mortar and technology constraints like the pump capacity can be taken into consideration.

4.4. On the existence of friction angle in mortar printing

Some optimisation strategies determining the feasibility of plastic or steel printing use a simple angular criterion, corresponding to the friction between two layers [15]. Using a simple analogy with Mohr Coulomb material, we have shown that the necessary condition for printing a horizontal layer of clay or concrete follows:

$$\beta = \frac{\tau_c}{\rho g h} > 1 \quad (14)$$

This equation is commonly fulfilled for current technologies. For example, the "infinite brick extrusion" has $\tau_c \simeq 1000 Pa$ and $h \simeq 0.02 m$. Clay-based materials also typically fall within that range. The pressing layer strategy has $\tau_c \simeq 100 Pa$ and $h \simeq 0.002 m$. The two strategies have a similar value for $\beta = 2.2$

Therefore, a local criterion is not enough to guarantee the printability, although the notion of critical angle is still used today to assess the printability of concrete cantilever. It is even possible to print horizontal cantilever.

The following experiment shown Fig. 23 illustrates the feasibility to stack layers horizontally, $\alpha = \pi/2$ (each layer is printed in a vertical plane).

A cylinder of 25 cm radius is printed on a vertical surface. The first layer is printed over staples that are protruding from the surface so it is mechanically anchored. The thickness of the layers is 4 mm and the target width is 20 mm, similar to the diameter of the nozzle. Eight layers were printed before the first failure occurs (32mm cantilever) resulting in the collapse of the lower part of

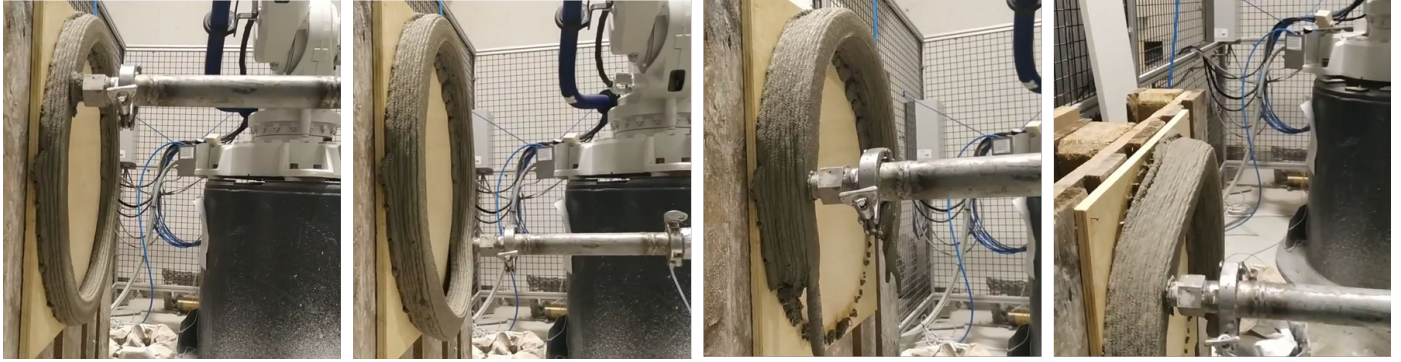


Figure 23: *From left to right:* Printing of a cylinder on a vertical surface. A local failure of the bottom part of the cylinder leads to a complete tearing of the lower part by pure tensile stress. The failure of the upper part of the cylinder occurs later at the anchoring of the first layer to the plate and is not due to the material itself.

the cylinder. The simple Finite Elements Analysis of a cylindrical shell shown on Fig. 24, gives an estimation of the critical Von Mises stress at the failure around 650 kPa. The upper part stayed in place while 7 more layers were printed for a total horizontal cantilever longer than 50 mm.

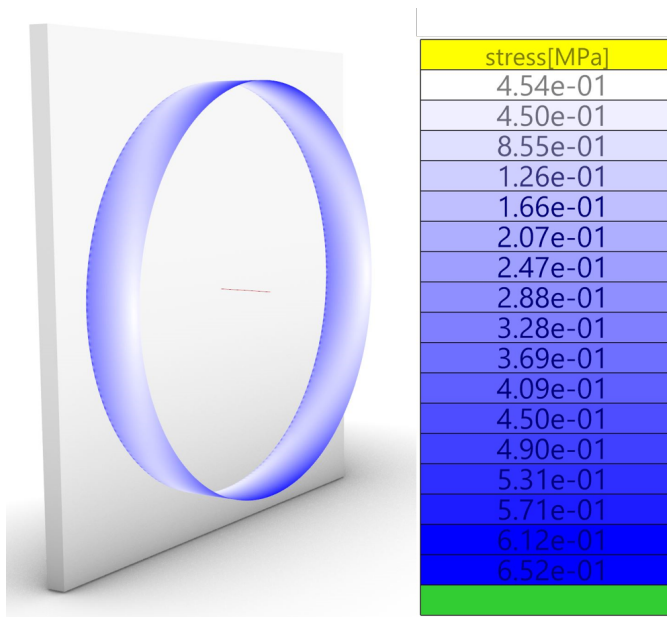


Figure 24: A finite elements analysis of a cylindrical shell. The figures shows the Von Mises stresses on the extrados of the shell under gravity for a thickness of 4cm.

The local criterion should therefore be assessed with several layers, and depends thus on thixotropy (the evolution of yield stress over time). The experimental test

shown in this article advocates for the use of more complex criterion than a simple angular criterion.

4.5. Framework for designing 3d printed structures

Table 2 below is a proposal of a framework for designing an object and its toolpath based on primitive boundary conditions, which is usually a constraint of the project, the targeted geometry and the technology in use. All geometries leading to structures working as much as possible in compression in the end. They are divided in three categories starting from a linear boundary condition, or a linear crossing from one point to the other. The form of the crossing will be that of an arch (pointed, circular, segmental, parabolic, etc.). The second category of geometries is obtained by translation of the previous arch, resulting in a barrel vault. The last follows a rotation of the same arch resulting in a dome (faceted or not).

The toolpath for the printing process can be generated from these geometries, taking into account the degrees of freedom of movement of the printing equipment and the control capacity of the printing parameters such as printing speed V_r and mortar flow rate Q . As mentioned before, the main common slicing strategies are a horizontal slicing, a constant angle slicing or a slicing fitting the geometry with a constant layer thickness for instance.

		BOUNDARY	FORM	SLICING		
				HORIZONTAL	CONSTANT ANGLE	CUSTOMIZED
ROTATED	LINEAR			• 3 axes	• 4 axes	• 6 axes • Speed control
	TRANSLATED			• 3 axes	• 3 axes	• 6 axes • Speed control
ROTATED	CIRCULAR			• 3 axes (+1) • Speed and Flow control	• 6 axes • Speed and Flow control	• 6 axes • Speed and Flow control
	FACETED			• 3 axes (+1) • Speed and Flow control	• 3 or 6 axes • Speed and Flow control	• 6 axes • Speed and Flow control
		etc.				

Table 2: Design framework for concrete 3d printing

4.6. Proof of concept - 3D printing of a barrel vault

This experiment is conducted using an extrusion head developed by XtreeE, mounted on a ABB 6-axis robotic arm (IRB-6620). The robotic path is programmed using HAL robotics plugin for Grasshopper, so that all the print parameters (robot speed V_r , concrete flow rate Q_c and additive flow rate) can be set beforehand or modified during the process.

The Nubian vault in Fig. 25 is printed as a proof of concept of a formwork-free concrete vault. The shape is generated as the funicular of its self-weight so the final geometry is fully in compression. In the main part of the vault, the slicing follows a constant angle of 40° . In the transition part, the layer inclination varies from 0° (first layer) to 40° . During the printing process, the extrusion is always tangent to the surface of the vault (see Fig. 25 right) so no local cantilever can appear between layers (criterion f^0 of pure shear stress). The feasibility of printing with a high inclination angle have been demonstrated in the previous part.

Due to the geometry and the slicing strategy, the length of the layers constantly increases from the first layer to the last one of the transition part. It then remains constant in the main part. The concrete flow Q_c is set once per layer with the minimal value of the pump set for the first layer

(the shortest) and the maximum value set for the last one.

Fig. 26 shows the local thickness of the layers of the vault. In the transition part, significant differences exist in a same layer (from 0.8 mm to 8 mm) due to the change in inclination and the need to go from a horizontal layer to a 40° angle. In the main part, even if the layer's length and inclination is constant, the thickness slightly changes due to the vault geometry and the slicing strategy (with a difference around 3 mm between the minimum and maximum). In order to keep the width of the layer d constant everywhere, the robot speed v_r has to be adjusted locally based on the thickness h of the layer and following Eq. 7.

Finally, from the printing speed and the length of the layers, we can compute the inter-layer time Δt and extract its bounds Δt^- and Δt^+ . The experience shows that with the mortar formulation used and the geometry of the vault, a $\Delta t^- > 9s$ is suitable for a successful print.

5. Conclusion

This paper is an attempt at giving directions for exploration of concrete 3d printing design space following examples of masonry structures that were built centuries ago without any temporary support. Hence, limiting the costs, the delays of construction and the wastes after completion. By identifying and classifying masonry strategies

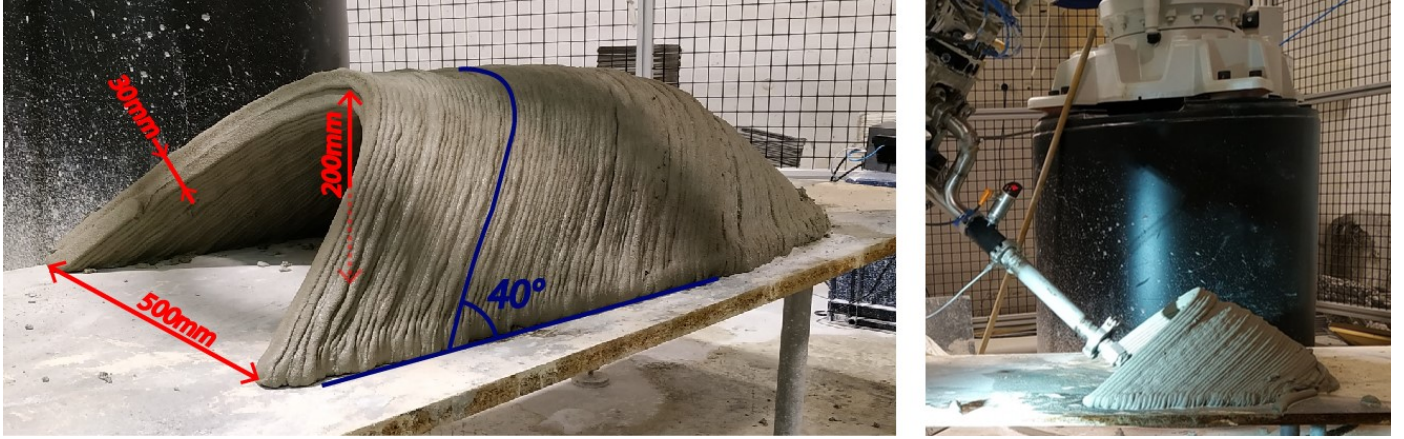


Figure 25: Example of a 3d printed Nubian vault where the slicing of the layers is made with a constant angle of 40° with the horizontal, and the printing head is always tangent to the vault surface.

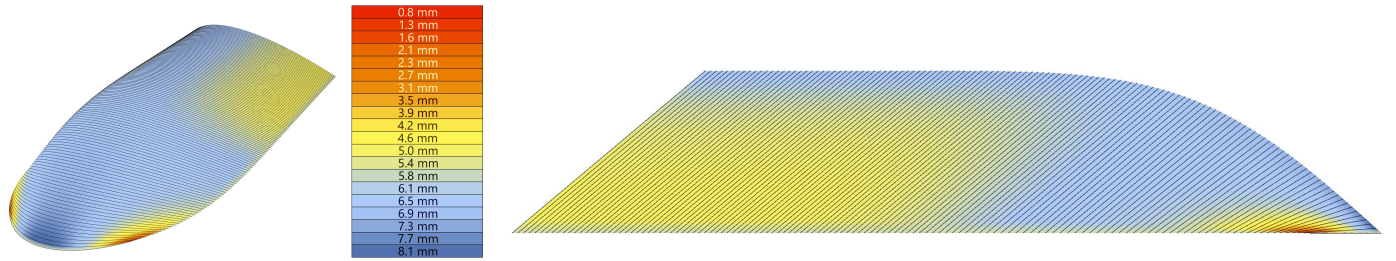


Figure 26: Thickness of the layers of a 3d printed Nubian vault. The thickness varies substantially within a same layer, especially in the transition part of the vault (first part), due to the continuous increase in the layer's inclination.

for creating cantilever, it is easier to target which parameters to play with when shifting to concrete printing.

If we refer to Duballet's classification of mortar 3d printing processes [29], this work fits the following criteria: an object scale of a meter (x_o^1), an extrusion scale less than 5cm (x_e^0 and x_e^1) and no assembly (a^0) or assembly of printed elements (a^1). The criteria for support conditions has already been mentioned in this paper, and developed alongside new criteria for additive manufacturing processes - the continuity of the layers and the initial stress state of the material. With the latter, we showed the advantage of inclining the layers over the creation of local corbels to generate global cantilever. And we detailed how these strategies are linked to the material used and the equipment available.

Finally, and based on previous statements, some guidelines for generating toolpaths, and some tools to validate

them have been proposed, in an attempt to broaden the range of printable geometries. To go further, a better understanding of the fresh material properties is necessary. For instance, characterisation tests must be developed to measure the initial yield stress τ_0 and the structuration rate A_{thix} of the material exiting the nozzle. From these data, new and more accurate form-finding process can be imagined, taking into account the fabrication process and the material property gradient.

5.1. Notations

Q is the concrete volumic flow [m^3/s]

V_r is the robot speed [m/s]

h is the layer height [m]

d is the layer width [m]

l is the total layer length [m]

μ is the concrete viscosity [P]

$\dot{\gamma}$ is the shear rate [s^{-1}]

τ is the actual shear stress while τ_0 is the initial yield stress and τ_c is the actual yield stress [Pa]

Δt is the inter-layer time [s]

6. Acknowledgement

The authors gratefully acknowledge the PhD funding of l'École des Ponts ParisTech and of its technological platform, Build'in, as well as the DiXite project, part of I-SITE Future initiative.

Appendix A. Critical angle of a layer before flow initiation

$$\begin{aligned}\tau &= \frac{F}{A} \sin(\alpha) \\ \sigma &= \frac{F}{A} \cos(\alpha)\end{aligned}\quad (\text{A.1})$$

By reporting in equation (1), it yields :

$$\frac{F}{A} \sin(\alpha) < c + \frac{F}{A} \cos(\alpha) \tan(\phi) \quad (\text{A.2})$$

With $F = \rho g h d l$ and $A = d l$ and by introducing $\beta = \frac{c}{\rho g h}$ this relation becomes:

$$\sin(\alpha) - \cos(\alpha) \tan(\phi) < \beta \quad (\text{A.3})$$

We see that since $\sin(\alpha) < 1$ and $\cos(\alpha) \tan(\phi) > 0$, the relation is always true when $\beta > 1$ and in this case

$$\alpha_{max} = \frac{\Pi}{2}.$$

If $0 < \beta < 1$, we write:

$$\sin(\alpha) \cos(\phi) - \sin(\phi) \cos(\alpha) < \beta \cos(\phi) \quad (\text{A.4})$$

$$\sin(\alpha - \phi) < \beta \cos(\phi) \quad (\text{A.5})$$

$$\alpha < \phi + \arcsin(\beta \cos(\phi)) \quad (\text{A.6})$$

Thus the values of the critical angle α_{max} :

$$\alpha_{max} = \begin{cases} \phi + \arcsin(\beta \cos(\phi)) & \text{if } 0 < \beta \leq 1 \\ \frac{\Pi}{2} & \text{if } \beta > 1 \end{cases} \quad (\text{A.7})$$

References

- [1] C. Llatas, A model for quantifying construction waste in projects according to the European waste list, *Waste Management* 31 (2011) 1261–1276. URL: <http://www.sciencedirect.com/science/article/pii/S0956053X11000559>. doi:10.1016/j.wasman.2011.01.023.
- [2] M. Popescu, M. Rippmann, T. Van Mele, P. Block, Complex concrete casting: knitting stay-in-place fabric formwork, in: *Proceedings of the International Association for Shell and Spatial Structures (IASS) Symposium 2016, Tokyo, Japan, 2016*, pp. 1 – 9. ISSN: 2518–6582. URL: https://block.arch.ethz.ch/brg/files/POPESCU_2016_IASS_complex-concrete-casting-knitting-stay-in-place-formwork_1545049665.pdf.
- [3] R. Duballet, O. Baverel, J. Dirrenberger, Design of Space Truss Based Insulating Walls for Robotic Fabrication in Concrete, in: K. D. Rycke, C. Gengnagel, O. Baverel, J. Burry, C. Mueller, M. M. Nguyen, P. Rahm, M. R. Thomsen (Eds.), *Humanizing Digital Reality*, Springer, 2017, pp. 453–461. URL: <https://hal.archives-ouvertes.fr/hal-01592008>. doi:10.1007/978-981-10-6611-5_39.
- [4] Y. W. D. Tay, B. Panda, S. C. Paul, N. A. Noor Mohamed, M. J. Tan, K. F. Leong, 3d printing trends in building and construction industry: a review, *Virtual and Physical Prototyping* 12 (2017) 261–276. URL: <https://www.tandfonline.com/doi/full/10.1080/17452759.2017.1326724>. doi:10.1080/17452759.2017.1326724.
- [5] C. Gosselin, R. Duballet, P. Roux, N. Gaudillière, J. Dirrenberger, P. Morel, Large-scale 3d printing of ultra-high performance concrete – a new processing route for architects and builders, *Materials & Design* 100 (2016) 102–109. URL: <http://linkinghub.elsevier.com/retrieve/pii/S0264127516303811>. doi:10.1016/j.matdes.2016.03.097.
- [6] T. A. Salet, F. P. Bos, R. J. Wolfs, Z. Y. Ahmed, 3d concrete printing—a structural engineering perspective, in: *High Tech Concrete: where Technology and Engineering Meet*, Springer Cham, 2018, pp. 43–57. doi:10.1007/978-3-319-59471-2.
- [7] S. Bhooshan, T. Van Mele, P. Block, Equilibrium-aware shape design for concrete printing, in: K. D. R. et al. (Ed.), *Humanizing Digital Reality - Proceedings of the Design Modelling Symposium 2017*, Springer, Paris, 2017, pp. 493–508. doi:10.1007/978-981-10-6611-5_42.
- [8] A. Suiker, Mechanical performance of wall structures in 3d printing processes: Theory, design tools and experiments, *International Journal of Mechanical Sciences* 137 (2018). doi:10.1016/j.ijmecsci.2018.01.010.
- [9] R. Wolfs, F. Bos, T. Salet, Early age mechanical behaviour

- of 3d printed concrete: Numerical modelling and experimental testing, *Cement and Concrete Research* 106 (2018) 103–116. doi:[10.1016/j.cemconres.2018.02.001](https://doi.org/10.1016/j.cemconres.2018.02.001).
- [10] S. C. Joshi, A. A. Sheikh, 3d printing in aerospace and its long-term sustainability, *Virtual and Physical Prototyping* 10 (2015) 175–185. URL: <https://doi.org/10.1080/17452759.2015.1111519>. doi:[10.1080/17452759.2015.1111519](https://doi.org/10.1080/17452759.2015.1111519).
- [11] C. Chua, K. F. Leong, 3D Printing and additive manufacturing: Principles and applications (with companion media pack) - fourth edition of rapid prototyping, World Scientific, 2014. doi:[10.1142/9008](https://doi.org/10.1142/9008).
- [12] S. Cacace, E. Cristiani, L. Rocchi, A level set based method for fixing overhangs in 3d printing, *Applied Mathematical Modelling* 44 (2017) 446–455. URL: <http://linkinghub.elsevier.com/retrieve/pii/S0307904X17301002>. doi:[10.1016/j.apm.2017.02.004](https://doi.org/10.1016/j.apm.2017.02.004).
- [13] E. Barnett, C. Gosselin, Weak support material techniques for alternative additive manufacturing materials, *Additive Manufacturing* 8 (2015) 95–104. URL: <http://www.sciencedirect.com/science/article/pii/S2214860415000299>. doi:[10.1016/j.addma.2015.06.002](https://doi.org/10.1016/j.addma.2015.06.002).
- [14] J. Dumas, J. Hergel, S. Lefebvre, Bridging the gap: automated steady scaffoldings for 3d printing, *ACM Transactions on Graphics* 33 (2014) 1–10. URL: <http://dl.acm.org/citation.cfm?doid=2601097.2601153>. doi:[10.1145/2601097.2601153](https://doi.org/10.1145/2601097.2601153).
- [15] G. Allaire, C. Dapogny, R. Estevez, A. Faure, G. Michailidis, Structural optimization under overhang constraints imposed by additive manufacturing technologies, *Journal of Computational Physics* 351 (2017) 295–328. URL: <http://linkinghub.elsevier.com/retrieve/pii/S0021999117307015>. doi:[10.1016/j.jcp.2017.09.041](https://doi.org/10.1016/j.jcp.2017.09.041).
- [16] Architecture of continuity: from materiality to environment, 2019. URL: <http://www.iaacblog.com/programs/perpetual-city-spatial-notions-3d-printed-future/>.
- [17] L. Reiter, T. Wangler, N. Roussel, R. J. Flatt, The role of early age structural build-up in digital fabrication with concrete, *Cement and Concrete Research* 112 (2018) 86–95. URL: <http://www.sciencedirect.com/science/article/pii/S0008884617312930>. doi:[10.1016/j.cemconres.2018.05.011](https://doi.org/10.1016/j.cemconres.2018.05.011).
- [18] S. Lim, R. Buswell, T. Le, S. Austin, A. Gibb, T. Thorpe, Developments in construction-scale additive manufacturing processes, *Automation in Construction* 21 (2012) 262–268. URL: <http://linkinghub.elsevier.com/retrieve/pii/S0926580511001221>. doi:[10.1016/j.autcon.2011.06.010](https://doi.org/10.1016/j.autcon.2011.06.010).
- [19] N. Roussel, Rheological requirements for printable concretes, *Cement and Concrete Research* 112 (2018) 76 – 85. URL: <http://www.sciencedirect.com/science/article/pii/S000888461830070X>. doi:<https://doi.org/10.1016/j.cemconres.2018.04.005>.
- [20] J. Andres, T. Bock, F. Gebhart, W. Steck, First Results of the Development of the Masonry Robot System ROCCO: a Fault Tolerant Assembly Tool, in: *Automation and Robotics in Construction* Xi, Elsevier, 1994, pp. 87–93. URL: <https://linkinghub.elsevier.com/retrieve/pii/B9780444820440500163>. doi:[10.1016/B978-0-444-82044-0.50016-3](https://doi.org/10.1016/B978-0-444-82044-0.50016-3).
- [21] L. Piskorec, D. Jenny, S. Parascho, H. Mayer, F. Gramazio, M. Kohler, The Brick Labyrinth, in: J. Willmann, P. Block, M. Hutter, K. Byrne, T. Schork (Eds.), *Robotic Fabrication in Architecture, Art and Design 2018*, Springer International Publishing, Cham, 2019, pp. 489–500. doi:[10.1007/978-3-319-92294-2_37](https://doi.org/10.1007/978-3-319-92294-2_37).
- [22] S. Lim, R. A. Buswell, P. J. Valentine, D. Piker, S. A. Austin, X. D. Kestelier, Modelling curved-layered printing paths for fabricating large-scale construction components, *Additive Manufacturing* 12 (2016) 216 – 230. URL: <http://www.sciencedirect.com/science/article/pii/S2214860416301154>. doi:<https://doi.org/10.1016/j.addma.2016.06.004>.
- [23] Y. W. D. Tay, M. Y. Li, M. J. Tan, Effect of printing parameters in 3d concrete printing: Printing region and support structures, *Journal of Materials Processing Technology* 271 (2019) 261–270. URL: <http://www.sciencedirect.com/science/article/pii/S0924013619301293>. doi:[10.1016/j.jmatprotec.2019.04.007](https://doi.org/10.1016/j.jmatprotec.2019.04.007).
- [24] I. Mungan, J. F. Abel, Fifty years of progress for shell and spatial Structures, *International Association for Shell and Spatial Structures (IASS)*, 2011. ISBN: 978-1-907132-35-3. URL: https://hal.archives-ouvertes.fr/hal-00856863/file/Fifth_Decade_Motro.pdf.
- [25] E. G. Nawy, *Concrete Construction Engineering Handbook*, CRC Press, Carmel, NY, 1997.
- [26] A. Choisy, *L’art de bâtir chez les Byzantins*, Librairie de la Société anonyme de publications périodiques, 1883. URL: <https://gallica.bnf.fr/ark:/12148/bpt6k3414739b>.
- [27] J. Pegna, Exploratory investigation of solid freeform construction, *Automation in Construction* 5 (1997) 427 – 437. URL: <http://www.sciencedirect.com/science/article/pii/S0926580596001665>. doi:[https://doi.org/10.1016/S0926-5805\(96\)00166-5](https://doi.org/10.1016/S0926-5805(96)00166-5).
- [28] B. Khoshnevis, Automated construction by contour crafting—related robotics and information technologies, *Automation in Construction* 13 (2004) 5–19. URL: <http://linkinghub.elsevier.com/retrieve/pii/S0926580503000736>. doi:[10.1016/j.autcon.2003.08.012](https://doi.org/10.1016/j.autcon.2003.08.012).
- [29] R. Duballet, O. Baverel, J. Dirrenberger, Classification of building systems for concrete 3d printing, *Automa-*

- tion in Construction 83 (2017) 247–258. URL: <http://linkinghub.elsevier.com/retrieve/pii/S0926580516302977>. doi:10.1016/j.autcon.2017.08.018.
- [30] M. Deuss, D. Panozzo, E. Whiting, Y. Liu, P. Block, O. Hornung-Sorkine, M. Pauly, Assembling self-supporting structures, *ACM Transactions on Graphics - SIGGRAPH Asia* 2014 33 (2014) 214:1–214:10. doi:10.1145/2661229.2661266.
- [31] P. Block, M. Rippmann, T. Van Mele, D. Escobedo, A. Menges, B. Sheil, R. Glynn, M. Skavara, The armadillo vault: Balancing computation and traditional craft, in: *Fabricate 2017*, UCL Press, 2017, pp. 286–293. ISBN: 978–1–78735–000–7. URL: www.jstor.org/stable/j.ctt1n7qkg7.43.
- [32] P. Block, T. V. Mele, A. Liew, M. DeJong, D. Escobedo, J. A. Ochsendorf, Structural design, fabrication and construction of the Armadillo vault, *The Structural Engineer: journal of the Institution of Structural Engineer* 96 (2018) 10–20. ISSN: 1466–5123. URL: <https://dialnet.unirioja.es/servlet/articulo?codigo=6529582>.
- [33] M. Godio, I. Stefanou, K. Sab, Effects of the dilatancy of joints and of the size of the building blocks on the mechanical behavior of masonry structures, *Meccanica* 53 (2018) 1629–1643. URL: <http://link.springer.com/10.1007/s11012-017-0688-z>. doi:10.1007/s11012-017-0688-z.
- [34] G. E. K. Smith, *Italy builds; its modern architecture and native inheritance*. L'Italia costruisce, New York, Reinhold, 1955. URL: <http://archive.org/details/italybuildsitsmo00smit>.
- [35] H. J. Cowan, A history of masonry and concrete domes in building construction, *Building and Environment* 12 (1977) 1–24. URL: <http://www.sciencedirect.com/science/article/pii/S0360132377900026>. doi:10.1016/S0360-1323(77)90002-6.
- [36] J. F. Hall, Fun with stacking blocks, *American Journal of Physics* 73 (2005) 1107–1116. URL: <http://aapt.scitation.org/doi/10.1119/1.2074007>. doi:10.1119/1.2074007.
- [37] J. Sakarovich, Gaspard Monge founder of "constructive geometry", BTU, Cottbus, Cottbus, Germany, 2009, pp. 1293–1300. URL: <https://hal.archives-ouvertes.fr/hal-00712704>.
- [38] J. Ochsendorf, M. Freeman, *Guastavino Vaulting: The Art of Structural Tile*, reprint ed., Princeton Architectural Press, New York, 2014. ISBN: 978-1-61689-244-9.
- [39] M. Rippmann, L. Lachauer, P. Block, Interactive Vault Design:, *International Journal of Space Structures* (2012). URL: <https://journals.sagepub.com/doi/10.1260/0266-3511.27.4.219>.
- [40] M. Ashkan, Y. Ahmad, Persian Domes: History, Morphology and Typologies, *Archnet-IJAR : International Journal of Architectural Research* 3 (2009). doi:10.26687/archnet-ijar.v3i3.192.
- [41] J. Fitchen, *The construction of Gothic cathedrals : a study of medieval vault erection*, Chicago : University of Chicago Press, 1981. URL: <http://archive.org/details/constructionofgo00fitch>.
- [42] M. Brocato, L. Mondardini, A new type of stone dome based on Abeille's bond, *International Journal of Solids and Structures* 49 (2012) 1786–1801. URL: <http://www.sciencedirect.com/science/article/pii/S0020768312001382>. doi:10.1016/j.ijsolstr.2012.03.036.
- [43] M. Brocato, L. Mondardini, Geometric methods and computational mechanics for the design of stone domes based on Abeille's bond, in: C. Ceccato, L. Hesselgren, M. Pauly, H. Pottmann, J. Wallner (Eds.), *Advances in Architectural Geometry 2010*, Springer Vienna, 2010, pp. 149–162. ISBN: 978–3–7091–0309–8.
- [44] V. Loing, Stereotomy and computer vision for robotic construction of complex masonry structures., Ph.d. thesis, Université Paris-Est Marne la Vallée, 2019. URL: https://www.researchgate.net/publication/337655296_Stereotomie_et_vision_artificielle_pour_la_construction_robotisee_de_structures_maconnees_complexes.
- [45] M. Betti, Numerical modeling of the structural behavior of brunelleschi's dome of santa maria del fiore, *International Journal of Architectural Heritage* (2015) 408–429. URL: https://www.academia.edu/21286718/Numerical_Modeling_of_the_Structural_Behavior_of_Brunelleschi_s_Dome_of_Santa_Maria_del_Fiore.
- [46] C. B. Costanzi, Z. Y. Ahmed, H. R. Schipper, F. P. Bos, U. Knaack, R. J. M. Wolfs, 3d Printing Concrete on temporary surfaces: The design and fabrication of a concrete shell structure, *Automation in Construction* 94 (2018) 395 – 404. URL: <http://www.sciencedirect.com/science/article/pii/S0926580517306556>. doi:https://doi.org/10.1016/j.autcon.2018.06.013.
- [47] E. Adiels, M. Ander, C. Williams, Brick patterns on shells using geodesic coordinates, in: *Interfaces: architecture.engineering.science: Proceedings of the IASS Annual Symposium 2017*, Hamburg, Germany, 2017, pp. 25–28. URL: http://publications.lib.chalmers.se/records/fulltext/254706/local_254706.pdf.
- [48] A. Prior, T. Svilans, J. Solly, Geodesically driven multi-axis clay deposition, *Innochain Network Journal* (2016). URL: https://issuu.Com/innochain/docs/network_journal_01_deliverable_2.1.
- [49] N. Ducoulombier, P. Carneau, Formwork-free 3d printing of a barrel vault with cementitious material, 2019. URL: <https://doi.org/10.5281/zenodo.3496964>. doi:10.5281/zenodo.3496964.
- [50] B. Zareiyan, B. Khoshnevis, Effects of interlocking on interlayer adhesion and strength of structures in 3d printing of concrete,

Automation in Construction 83 (2017) 212–221. doi:[10.1016/j.autcon.2017.08.019](https://doi.org/10.1016/j.autcon.2017.08.019).

- [51] N. Roussel, P. Belin, H. Bessaies Bey, W. Zuo, E. Keita, Weak bond strength between successive layers in extrusion-based additive manufacturing: measurement and physical origin, Cement and Concrete Research 123 (2019). doi:[10.1016/j.cemconres.2019.105787](https://doi.org/10.1016/j.cemconres.2019.105787).